Journal of Zhejiang University-SCIENCE A (Applied Physics & Engineering)
ISSN 1673-565X (Print); ISSN 1862-1775 (Online)
www.jzus.zju.edu.cn; link.springer.com
E-mail: jzus_a@zju.edu.cn

Numerical study on failure propagation between two closely spaced tunnels*

Gang ZHENG, Rui ZHU, Ji-bin SUN, Tian-qi ZHANG†‡, Jing-bo TONG, Rui-kun WANG, Yu DIAO

School of Civil Engineering, Tianjin University, Tianjin 300072, China

†E-mail: tianqizhang@tju.edu.cn

Received Nov. 4, 2020; Revision accepted May 6, 2021; Crosschecked Oct. 20, 2021

Abstract: An increasing number of engineering accidents have shown that the failure of a tunnel can propagate to a neighbouring tunnel. However, due to the complex interaction between the failed tunnel structure and the soil medium, the mechanism by which the failure is propagated between two closely spaced tunnels remains unclear. In this study, the coupled Eulerian-Lagrangian (CEL) modelling technique was adopted to investigate the influence of a failed tunnel (FT) on an adjacent tunnel, which was termed an "influenced tunnel" (IT). The safety of the IT was analysed in detail under different circumstances, such as different failure positions of the FT, different failure degrees of the FT, and different spatial relationships between the two tunnels. The simulation results indicated that the most adverse case may occur when the two tunnels are arranged as offsets and the IT is the upper tunnel. Under this circumstance, significant shear deformation may occur in IT because IT is located at the shear band of the FT.

Key words: Failure propagation; Closely spaced tunnels; Coupled Eulerian-Lagrangian (CEL)
https://doi.org/10.1631/jzus.A2000502 **CLC number:** U458

1 Introduction

With the rapid development of the economy and functional zoning of urban space, subway construction has become an important index for evaluating the level of urbanization worldwide. In China, subway transportation has become a mainstay of urban public transport, especially in first-tier cities such as Beijing and Shanghai (Huang et al., 2020, 2021).

However, increasingly devastating engineering accidents have occurred during subway construction. For example, the collapse of a tunnel in the Nanjing Metro Line 2 caused severe ground subsidence (Yang, 2011); the accident that occurred during the construction of Metro Line 2 in Foshan caused the deaths of 11 people and the direct economic loss of 50 million CNY (Department of Emergency Management of Guangdong Province, 2019). These accidents led to great financial losses and severe social impacts.

Extensive pioneering works have been done to investigate the mechanism behind the failure of the tunnels. Seidenfuß (2006) collected more than 110 cases of accidents in practical engineering and analyzed the failure mechanism of the tunnel face, as in tunnel collapse accidents in London and Munich. HSE (1996) summarized different sorts of face stabilities of the tunnel, including the collapse on the surface and collapse under the ground. Chambon and Corté (1994) conducted centrifuge model tests to study the stability of the tunnel face in sand. Atkinson and Potts (1977) conducted centrifuge model tests to study the face stability of the circle tunnel section and analyze the influence of the linings. Numerical models were also widely adopted to study

‡ Corresponding author
* Project supported by the National Natural Science Foundation of China (Nos. 41630641 and 51808387)
ORCID: Tian-qi ZHANG, https://orcid.org/0000-0003-0145-973X

the stability of tunnels. Zheng et al. (2018) used the Eulerian finite model for stability analysis of circular tunnels in undrained clay. Yamamoto et al. (2011) focused on the stability of a square tunnel in cohesive-frictional soils subjected to surcharge loading. As for study of progressive failure of the tunnels, Yin et al. (2020) analyzed the progressive face failure of a shield tunnel in sand using the coupled discrete element method and the finite difference method. Cui (2017) performed small-scale model tests to study the trigger mechanism of progressive failure in shield tunnels. Zheng et al. (2020) adopted numerical simulations to investigate the propagation mechanism of the domino-like failure in shield tunnels. Basically, these studies mainly focused on the failure of a single tunnel.

Nowadays, with the utilization of the underground space, the distance between tunnels is becoming smaller, especially in built-up regions and, in such circumstances, the failure of a tunnel may pose a threat to the safety of a neighbouring tunnel. For example, in the accident on Shanghai Metro Line 9, 20 rings of segments failed in the up-line tunnel, which led to the excessive deformation of segments in the neighbouring down-line tunnel (Lu et al., 2007). Similarly, in Shanghai Metro Line 4 (Fang et al., 2009), the right line tunnel failed during the excavation of the connecting passage (Fig. 1a), which gave rise to the collapse of the left line tunnel (Fig. 1b). In general, compared to the failure of a single tunnel, the cascading failure of a multi-tunnel system will be more catastrophic. The studies on the interaction between two crossing tunnels were mostly under the circumstances of normal operating conditions (Zhang, 2016; Jin YF et al., 2019). However, little research has been conducted on how the failure of one tunnel can affect a neighbouring one, and the mechanism by which the failure is propagated between closely spaced tunnels remains unclear.

In this study, we describe numerical simulations carried out to study the influence of a failed tunnel (FT) on an adjacent tunnel, referred to as an "influenced tunnel" (IT). To simulate the complex interaction between the failed tunnel structure and the soil medium, a coupled Eulerian-Lagrangian (CEL) modelling approach was adopted. The safety of the IT was analyzed in detail under different circumstances, including different failure positions of the FT, different failure degrees of the FT, and different spatial relationships between the two tunnels. Based on the simulation results, some suggestions are provided for preventing the cascading failure of two closely spaced tunnels.

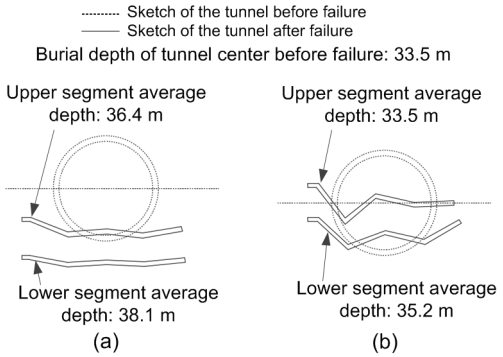

Fig. 1 Accidents on Shanghai Metro Line 4
(a) Failure of segments in right line tunnel; (b) Failure of segments in left line tunnel

2 Numerical model

2.1 Implementation of CEL modelling

The classical finite element (FE) methods are mostly based on a Lagrangian formulation and are not suitable for solving geotechnical problems with large deformation due to excessive distortion of the FE-mesh. Hence, many numerical approaches have been implemented to overcome these problems, such as smoothed particle hydrodynamics (SPH), arbitrary Lagrangian-Eulerian (ALE), and CEL (Arrazola and Özel, 2010; Jin YF et al., 2018a; Yin et al., 2018; Jin Z et al., 2019). In this study, the CEL method was implemented due to a stable calculating result and a higher computational efficiency in massive grid computation (Qi et al., 2018).

In general, there are two ways to describe the movement of continuum bodies: the Lagrangian description and the Eulerian description. In the simulation using Lagrangian formulation, the movement of the continuum is described as a function of material coordinates and time. The nodes of Lagrangian elements move together with the material. In the Eulerian analysis, the movement of the continuum is described as a function of the spatial coordinate and time. In the Eulerian analysis, the Eulerian reference mesh is needed to trace the motion of material and

the material can move freely through the Eulerian mesh.

The CEL method combined the advantages of both the Eulerian and Lagrangian analyses. In the numerical simulation using the CEL method, the flow of Eulerian material is tracked by computing the Eulerian volume fraction (EVF) of the mesh. Each Eulerian element was designated a percentage, which represents the portion of that element filled with a material. Specifically, if the element is full of material, EVF=1; if there is no material in the element, EVF=0. The contact between Eulerian materials and Lagrangian materials was implemented by the "general contact" algorithm, which was based on the penalty contact method (Qiu et al., 2011; Qiu and Grabe, 2012). With this method, small penetration of Eulerian material into Lagrangian elements was allowed. The contact force would increase linearly with the penetration distance.

Several benchmark calculations revealed that the CEL approach worked well in solving geotechnical problems with large deformations (Huo et al., 2016; Wu et al., 2017; Dai et al., 2018; Jin YF et al., 2018b; He et al., 2019). In this study, a series of "2D" models are described using the CEL method in ABAQUS^{TM} commercial software (Version 2016) to study the influence of the failure of a tunnel on an adjacent tunnel.

Fig. 2 shows an example of the 2D model, in which two parallel tunnels were considered. In the CEL method, only 3D modelling was permitted. Therefore, the analysis of only one element length in the out-of-plane direction was performed. In this model, local failure was set in the FT. The process of local failure was modelled by removing the corresponding failed segment in the FT. Soil was modelled as Eulerian material, and 3D linear brick hexahedron elements with reduced integration (EC3D8R) were used. The tunnel consisted of several segments that were modelled by Lagrangian elements. The joints between segments were simulated by tensile springs, shear springs, and bending springs (the properties of segments and joints will be discussed later). Zero velocity constraint conditions were applied normal to the bottom and the vertical boundaries in the Eulerian domain to avoid soil flowing out of the model.

The simulation process can be divided into two steps:

Step 1: activate the initial boundaries. In this step, all the segments and joints functioned well, and both tunnels were in normal working condition. The EVF of the Eulerian elements inside the tunnel was set to 0 because there was no soil leaking into the tunnel in this step. A void layer whose EVF was 0 was set at the top of the model to prevent the soil from flowing out of the model, which may cause the loss of material (Fig. 2). The entire model was placed in a gravitational field of 1g, where g is the gravitational acceleration. A coefficient of lateral earth pressure K_0=0.46 based on Jack's equation (K_0 =1−sinφ_c', in which φ_c' was the effect friction angle, taken as 33°) was adopted in the model. The initial stress condition of the Eulerian element was adopted in equilibrium with gravity.

Step 2: deactivate the two joints that were connected with the failed segment to trigger local failure in the FT (the deactivation operation was achieved by changing field variables in ABAQUS). Then, the soil began to leak into the tunnel from the local failure position. The EVF of the Eulerian elements inside the FT varied between 0 and 1, and the soil stress near the IT may change, giving rise to variations in the internal forces of the joints in the IT. This step simulated the process from the moment when local failure occurred in the FT to the moment when the internal forces of the joints in the IT finally became stable.

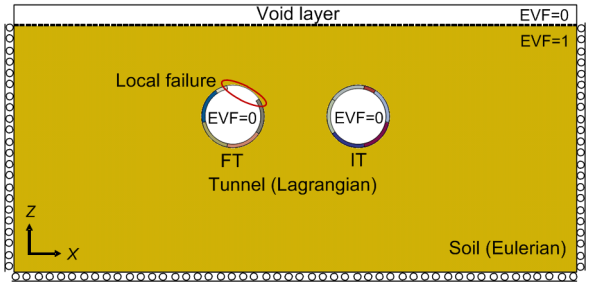

Fig. 2 Schematic of the 2D CEL model

2.2 Simulation of soil behaviour

For simplicity, the tunnels were assumed to be built in dry sand. The hypoplastic model was implemented to model the behaviour of soil considering its good fitness in modelling the nonlinear behaviour of granular soils (Ng et al., 2015). In this model, the version including the intergranular strain concept of Niemunis and Herle was used (Niemunis and Herle,

1997). This model contains eight basic parameters (φ_c': critical state friction angle; h_s: granulate hardness; n: hardness exponent; e_{d0}: minimum void ratio at zero pressure; e_{c0}: critical state void ratio at zero pressure; e_{i0}: maximum void ratio at zero pressure; α and β: parameters governing the dilation angle and shear stiffness of soil) that describe the general characteristics of soil (e.g. dilatancy, contractions, different stiffnesses of loading and unloading, as well as the dependency of the stiffness on the pressure and void ration) and five additional parameters (m_R: parameter controlling initial shear modulus upon 180° strain path reversal and in initial loading; m_T: parameter controlling the initial shear modulus upon 90° strain path reversal; R: size of the elastic range; β_r and χ: parameters controlling the rate of degradation of the stiffness with strain) to describe the small-strain and strain-dependency behaviour of soil. A typical parameter of the Hochstetten sand which was adopted for the simulation is shown in Table 1 (Herle and Gudehus, 1999).

Table 1 Hypoplastic constitutive parameters of Hochstetten sand

Parameter	Value	Parameter	Value	Parameter	Value
γ (t/m^3)	1.5	e_{c0}	0.95	m_T	2
φ_c' (°)	33	e_{i0}	1.05	R	0.0001
h_s (MPa)	1500	α	0.25	β_r	0.5
n	0.28	β	1	χ	6
e_{d0}	0.55	m_R	5	d_r	0.84

γ: unit weight of soil; d_r: relative density

2.3 Simulation of tunnel structure

A schematic diagram of the tunnel is shown in Fig. 3. As shown in the figure, different joints and segments were named for the convenience of subsequent explanations. Each tunnel consisted of six segments (five standard blocks and one key block). The central angle of each standard block is 67.5°, and the central angle of each key block is 22.5°. The external diameter of each tunnel was 6.2 m, while the internal diameter of each tunnel was 5.5 m. The segments were assumed to be made of C50 reinforced concrete.

Two bolts with a nominal diameter of 30 mm and an ultimate bearing capacity of 800 MPa were used to connect the segments. The distance between the location of the bolts and the internal surface of the tunnels was set as 0.14 m. According to previous studies (Zeng and He, 2004; Li et al., 2015), the bearing capacity of a joint varies when it is in different bending directions (sagging moment and hogging moment). When the joint is in the state of sagging moment, the internal surface of the tunnel opens; when the joint is in the state of hogging moment, the external surface of the tunnel opens. A diagram of the two bending directions and the corresponding formulas of the envelope curve are shown in Fig. 3 (Cui, 2017).

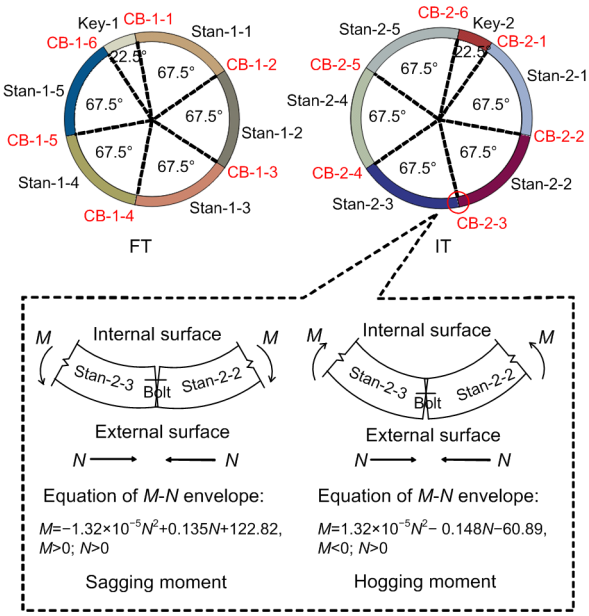

Fig. 3 Schematic diagram of the tunnel
M: bending moment (kN); N: axial force (kN/m)

According to previous studies, joints are the weakest part in shield tunnels, while segments can be in a relatively safe state when failure occurs (Geng et al., 2020; Zhang et al., 2020). Fully understanding this fact, only the failure behaviour of the joints was simulated, and the failure of the segments was neglected in this study (the computed bending moments in the segments are provided in Appendix A and indicate that the segments were indeed safe). The segments were modelled as elastic Lagrangian bodies that had an elasticity modulus of 34 500 MPa.

The tensile springs, shear springs, and bending springs of the joints were simulated with an elastic model when the internal force of the joint is within the ultimate bearing capacity. The parameters are shown in Table 2 (Liu et al., 2016). The ultimate

bearing capacity of the bending springs was related to the axial forces of the joint. When the axial force and bending direction of the joint were determined, the ultimate bearing capacity could be calculated with the formula shown in Fig. 3.

In this study, the behaviour of the joints was defined as follows. First, for the joints in the FT, under circumstance 1, if the internal force in any one of the three springs of the joint developed beyond its ultimate bearing capacity, the joint could not bear any bending moment; under circumstance 2, no matter how the internal force in the three springs of the joint developed, the joint could always undertake the corresponding force. Second, for the joints in the IT, the behaviour of the joints was the same as that of the joints in the FT under circumstances 2, which means all the joints in the IT could work properly.

Table 2 Parameters of springs

Type	Direction	Rigidity	Ultimate bearing capacity
Tensile spring	Axial	477 529 kN/m^2	754 kN/m
Shear spring	Tangential	182 896 kN/m^2	377 kN/m
Bending spring	Sagging	9167 kN/rad	
	Hogging	5416 kN/rad	

3 Model validation

Liu and Huang (2015) conducted a full-scale test to study the collapse capacity of straight joint segment tunnels. In the present study, this experiment was reproduced to verify the modelling method of the joints, which was discussed above.

As shown in Fig. 4, in the present model, the ring consisted of one key block, two adjoining blocks, two standard blocks, and one bottom block. The external radius of the ring was 6.2 m, and the internal radius was 5.5 m. The width of the ring was 1.2 m. The segments were constructed with C55 concrete, and the reinforcing steel bar had a stage of HRB 335. The longitudinal joint was connected by two bolts with a diameter of 30 mm and the strength of extension of the bolts was 800 MPa. Around the tunnel, 24 hydraulic jacks were adopted to simulate the load. The loading process was divided into two steps: first, the load around the tunnel was applied gradually from zero to the normal operation load; second, the vertical pressure was maintained while the lateral pressure was decreased until the ultimate state of the tunnel was reached.

A comparison of numerical simulation and experiment is shown in Fig. 5. Fig. 5a shows the vertical compressed deformation development of the failed tunnel. The trends of the elastic stage, plastic development stage, and plastic stage were well simulated, and the ultimate load in the numerical calculation was close to that in the experiment. Fig. 5b shows the development of the joint stretching value at 8° of the ring, and the calculation result agreed

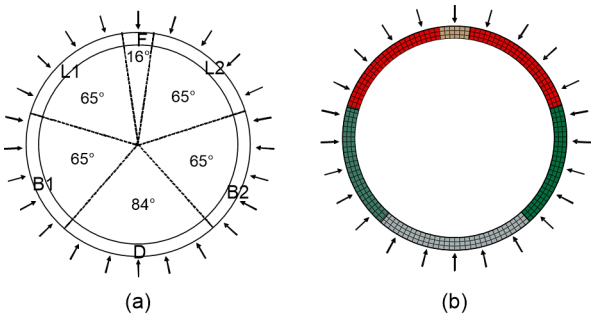

Fig. 4 Sketch of the tunnel

(a) Sketch of the tunnel in the experiment; (b) Sketch of the tunnel in the numerical calculation

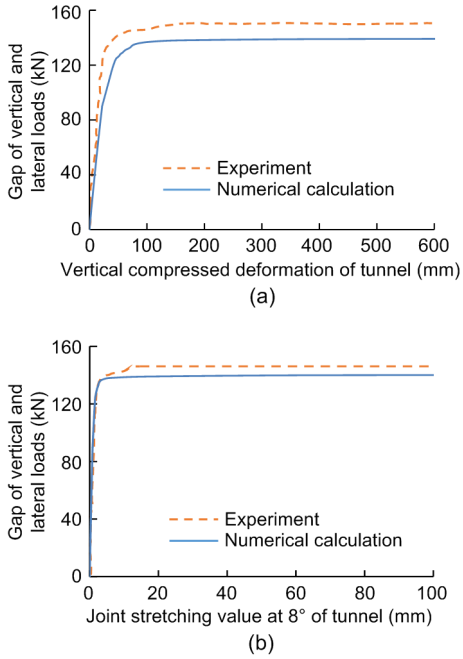

Fig. 5 Comparison of the numerical simulation and experiment

(a) Vertical compressed deformation of tunnel; (b) Joint stretching value at 8° of tunnel

well with the experiment. In general, the modelling method of the joints was deemed reasonable.

4 Analysis of the results

Two circumstances were considered here. Circumstance 1 only considered local failure (LF). In this circumstance, local failure occurred, and soil leaked into the FT from the failure position. All the joints functioned well during the failure process. Circumstance 2 considered progressive failure (PF). In this circumstance, not only would soil leak into the failed tunnel but also joints might fail during the failure process (the internal forces in the joints left the *M*-*N* envelope). The failure of the joints would probably induce the collapse of the tunnel. A schematic diagram of the two circumstances is shown in Fig. 6 (in the schematic diagram, local failure occurred at Stan-1-1). In practical engineering, LF corresponded to the situation in which effective measures were taken in time to prevent the collapse of the FT after local failure occurred. PF corresponded to the situation in which it was too late to take measures to protect the structure of the tunnel, and progressive failure occurred after local failure.

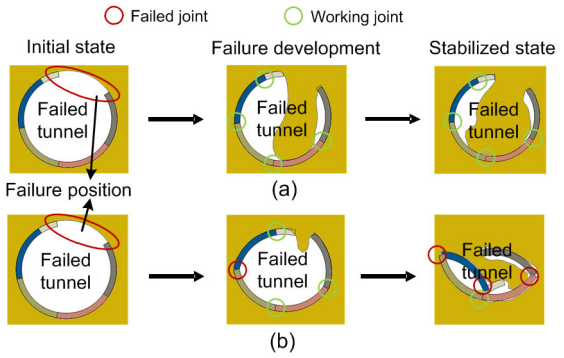

Fig. 6 Two circumstances considered after local failure occurred in the FT

(a) Circumstance 1: only considering local failure; (b) Circumstance 2: considering progressive failure

4.1 Sequence of joints that went into an unsafe state in the IT

According to the current design method of joints in shield tunnels, connecting bolts with identical strength levels and concrete with identical strength grades were used in the same tunnel. This design meant that all the circumferential joints had identical envelope lines of axial force and bending moments regardless of whether the joints were at the top or bottom of the tunnel. This design principle was effective and convenient when tunnels were constructed and served in a normal way. However, if one tunnel failed, whether the joints in the other tunnel could bear the corresponding changing load and remain safe was unclear. To illustrate this problem, the internal force development of the joints in the IT is shown in Fig. 7 when the failure position was Stan-1-1 and the circumstance of PF occurred in the FT. In Fig. 7, the internal forces of different joints in the IT are marked with different symbols. For instance, CB-2-1 is marked with a square, and CB-2-2 is marked with a circle. The same symbols are connected with straight lines to show the internal force change of the joints. When the internal forces of the joints developed within the envelope, solid lines are used to connect the figures. When the internal forces left the envelope, the connecting lines are shown as dashed lines. An unsafe state was defined as a state in which the internal force of a joint in an IT left the envelope, and a joint in an unsafe state was named an unsafe joint. For instance, the unsafe joints were CB-2-2, CB-2-3, and CB-2-6 (which are marked with circles) in Fig. 7.

As shown in Fig. 7, different joints in the IT showed different working states. For example, some of the joints went into an unsafe state (CB-2-2, CB-2-3, and CB-2-6), while other joints remained safe. In addition, there were also differences between the internal force developments of these unsafe joints. First, the unsafe joints went into an unsafe state at different moments. For example, joint CB-2-2 was the first to go into an unsafe state in the IT, followed by CB-2-3 and CB-2-6. Second, joints such as CB-2-6 went into an unsafe state to a small degree, while other joints such as CB-2-3 went into an unsafe state to a large degree.

Fig. 7 only shows the internal force development of the joints in the IT when the spatial relationship of the two tunnels was parallel. However, the two tunnels can also be arranged as offsets or overlaps. To exhibit practical engineering in a comprehensive way, different spatial relationships of the two closely spaced tunnels were simulated (Table 3).

Because parallel tunnels can be taken as symmetrical structures, only the case in which the left tunnel failed was simulated. For the offset and overlap tunnels, the situation in which the upper tunnel failed (such as Offset-1 and Overlap-1) and the situation in which the lower tunnel failed (such as Offset-2 and Overlap-2) were considered, respectively. In general, there were five different cases. In each case, the burial depth of the upper tunnel was 1*D*, and the distance between the centers of the two tunnels was 2*D* (*D* is the tunnel diameter).

In addition, the failure position may not only be at Stan-1-1, as local failure may also occur at any position in the FT. Hence, different failure positions in the FT were also simulated. Fig. 8 shows the possible failure modes of the FT when local failure occurred at different positions (Key-1, Stan-1-1, Stan-1-2, Stan-1-3, Stan-1-4, and Stan-1-5). Different local failure positions are marked with different numbers (1), (2), (3), (4), (5), and (6).

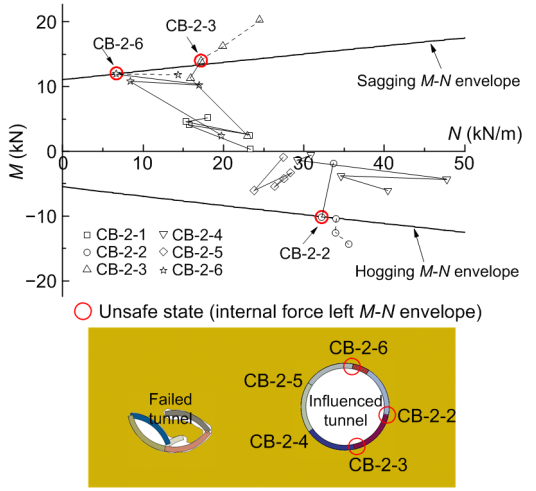

Fig. 7 Internal force development of the joints in the IT when Stan-1-1 failed in FT

Sequence of joints that went into an unsafe state: CB-2-2→CB-2-3→CB-2-6

Table 3 Introduction of different cases

Case	FT	IT	Buried depth	Central distance
Parallel	Left	Right	1*D*	2*D*
Offset-1	Upper	Lower		
Offset-2	Lower	Upper		
Overlap-1	Upper	Lower		
Overlap-2	Lower	Upper		

Fig. 8 shows the sequence of joints that went into an unsafe state in the IT in the Parallel case. The working states of each joint in the IT are shown with 12 blocks that corresponded to different failure modes of the FT (six for LF and six for PF). Blocks with no numbers represent the joints that remained safe in the corresponding failure modes, while blocks with numbers represent the joints that were in an unsafe state. The numbers indicate the sequence of joints that went into an unsafe state. For example, for the 12 blocks that indicated the working states of joint CB-2-6, the block located in the first column of the first line indicated that joint CB-2-6 remained safe when the failure position was Key-1 if the FT was in circumstance 1. The block located in the second column of the second line is marked with number (3). This mark indicates that joint CB-2-6 was the third joint to go into an unsafe state when the failure position was Stan-1-1 if the FT was in circumstance 2.

As illustrated in Fig. 8, in LF, the internal force development of all joints in the IT was within the *M*-*N* envelope. In PF, joint CB-2-3, which was located at the invert of the IT, and joint CB-2-2, which was located at the springline of the IT, were the first two joints to go into an unsafe state. This result means that the joints located at the invert and springline of the tunnel should be given more attention in the Parallel case.

The working states of the joints in the IT were compared when local failure occurred at the same position of the FT in the two circumstances. It is found that joints CB-2-2, CB-2-3, and CB-2-6 can always remain safe in LF, while these joints may go into an unsafe state in PF when some positions fail in the FT. This result illustrates that different circumstances may influence the working states of the joints, especially those located at the invert and springline of IT in the Parallel case.

When the two tunnels were arranged as offsets, all the joints in IT can stay safe in the case Offset-1, while some joints may go into an unsafe state in the case Offset-2. Fig. 9 shows the sequence of joints that went into an unsafe state in the IT for Offset-2. In LF, joint CB-1-3, which was located at the toe of the IT, and joint CB-1-4, which was located at the invert of the IT, were the first two joints to go into an unsafe state; in PF, the first two joints that went into an unsafe state were similar to those in LF. This

result means that the invert and the toe of the IT should be emphasized in the case of Offset-2.

When the two tunnels were arranged as overlaps, all the joints in IT can stay safe in the case Overlap-1, while some joints may go into an unsafe state in the case Overlap-2. Fig. 10 shows the sequence of joints that went into an unsafe state in the IT in the case of Overlap-2. In LF, joint CB-1-4, which is located at the invert of the IT, and joint CB-1-5, which is located at the springline of the IT, were the first two joints to go into an unsafe state. In PF, the first two joints that went into an unsafe state were similar to those in LF. This result revealed that the invert and the springline of the IT should be given more attention.

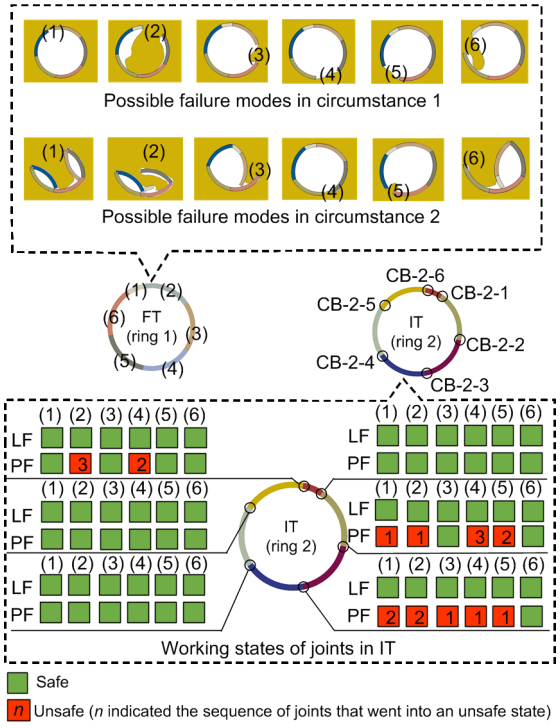

Fig. 8 Sequence of joints that went into an unsafe state in the Parallel case

(1)–(6) show six positions where local failure may occur. LF: only considering local failure; PF: considering progressive failure

From Figs. 8–10, conclusions can be drawn when comparing the working states of the joints in the IT under different circumstances. First, the sequences of the first two joints that went into an unsafe state in the IT were similar in different circumstances in each case. For example, for Overlap-2, the first two joints in the IT that went into an unsafe state were CB-1-4 and CB-1-5 regardless of whether the FT was in LF or PF. Second, different circumstances may influence the number of unsafe joints in each case. The number of unsafe joints of the IT may be larger in PF than in LF in each case. For example, in the Parallel case, all the joints remain safe in LF, while some joints (CB-2-2, CB-2-3, and CB-2-6) can be unsafe when local failure occurs at some positions in the FT in PF.

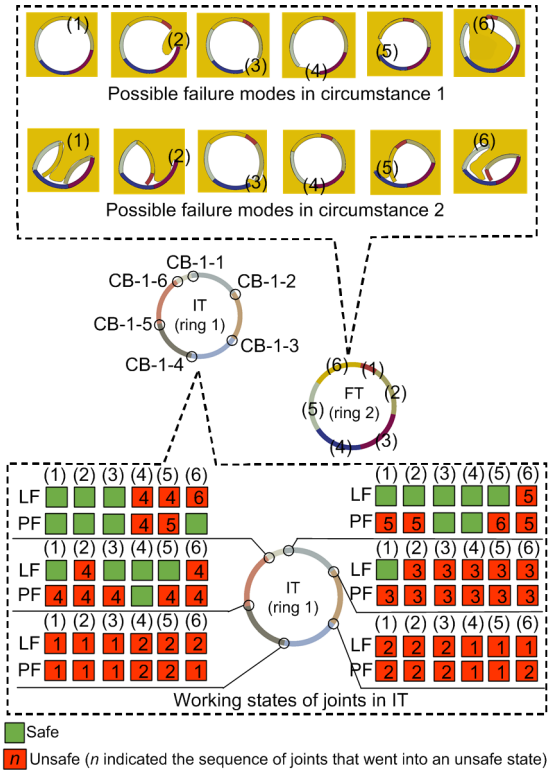

Fig. 9 Sequence of joints that went into an unsafe state in the case of Offset-2

4.2 Degree to which joints went into an unsafe state in the IT

The above study showed the working states of the joints in the IT. It also revealed that different unsafe joints went into an unsafe state at different moments in each case. However, as mentioned above, the difference between unsafe joints in each case was not only the sequence of joints that went into an unsafe state but also the degree to which different unsafe joints left the envelope. Many scholars

(Bi et al., 2014; Li et al., 2015; Liu and Huang, 2015) have reached the conclusion that flexural failure is the primary reason why joints lose function in shield tunnels. On that basis, the safety factor of joints can be evaluated by the flexural strength and the bending moments.

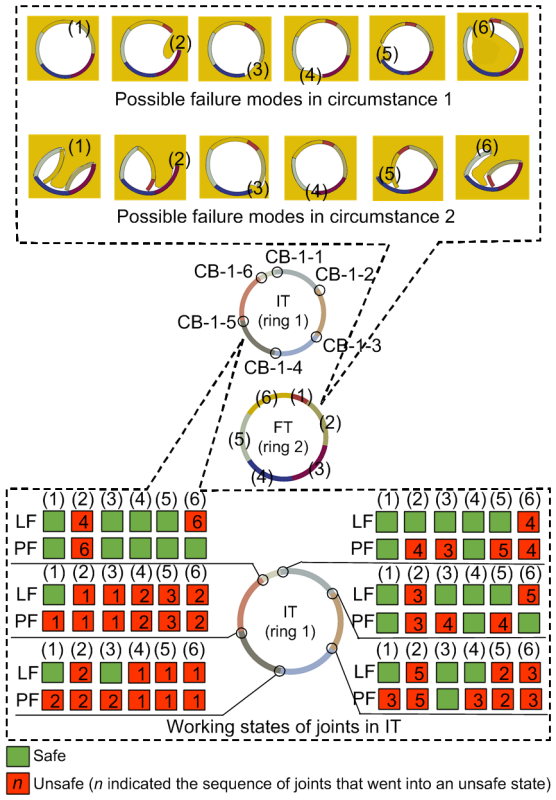

Fig. 10 Sequence of joints that went into an unsafe state in the case of Overlap-2

A schematic diagram of the safety factor of joints in the IT is shown in Fig. 11. The curve *OAB* represents the internal force development of a joint in the IT. Point *A* was a discretional point in the curve *OB*, and a straight line through point *A* was drawn perpendicular to the *X* axis. The intersection of the straight line and the envelope line was point *P*, and the intersection of the straight line and the *X* axis was point *Q*. The line segment *AQ* (M_1) represented the current bending moment of the joint, while the line segment *PQ* (M_2) represented the flexural strength of the joint. The specific values of M_2 and M_1 were defined as K_a. The value of K_a changed as point *A* varied along the curve *OB*, and the minimum value of K_a (which is also called *K* in Fig. 11) was defined as the safety factor of the joint. The range of values of *K* was 0 to positive infinity. The larger *K* is, the safer the joint can be. If *K* was between 0 and 1, the value of the flexural strength of the joint was smaller than that of the bending moment, and the joint was unsafe. If *K* was larger than 1, the flexural strength of the joint was sufficiently strong to resist the bearing moment.

Fig. 12 shows the safety factor of the joints in the IT in the case of Parallel. In LF, the smallest safety factor was 1.33, and joint CB-2-2, which was located at the springline of the IT, and joint CB-2-3, which was located at the invert of IT, were the two joints with the smallest safety factors in most cases. In PF, joint CB-2-3, which was located at the invert of the IT, was the joint with the smallest safety factor, and the smallest safety factor was 0.54. In practical engineering, the invert and springline of the IT should be enhanced in the design stage.

Comparing the safety factors of the joints in the IT under different circumstances shows that the safety factors of the joints in LF were larger than those in PF. This result indicated that the timely prevention of progressive failure of the FT can obviously increase the safety factor of the joints in the IT in the Parallel case.

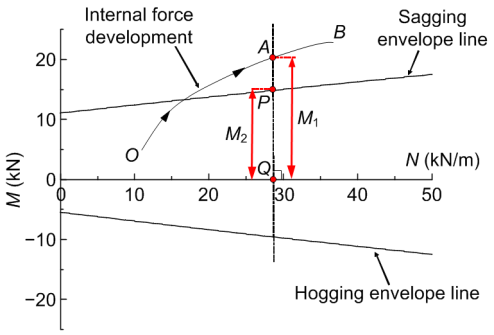

Fig. 11 Diagram of the safety factor of the joints in ITs
Safety factor *K* is the minimum of K_a (K_a=M_2/M_1)

When the two tunnels were arranged as offsets, in the case Offset-1, the joints in IT had sufficient redundancy of security (the safety factors ranged from 1.23 to 10.20). While in the case Offset-2, some joints in IT may go into the unsafe state. The safety factors of the joints in the IT for Offset-2 are shown in Fig. 13. In LF, joint CB-1-4, which was located at the invert of the IT, had the smallest safety

factors in most cases, and the safety factors of CB-1-4 ranged from 0.25 to 0.81 when local failure occurred at different positions in the FT. In addition, joint CB-1-2, which was located at the springline of the IT, and joint CB-1-3, which was located at the toe of the IT, should also be given more attention. The safety factors of those two joints were approximately 0.5. In PF, joint CB-1-4 had the smallest safety factors in most cases, ranging from 0.22 to 0.32. The safety factors of joints CB-1-2 and CB-1-3 were smaller in PF than in LF. This result revealed that the joints located at the springline, toe, and invert of the IT may leave the envelope to a large degree, and these joints should be taken seriously in the case of Offset-2.

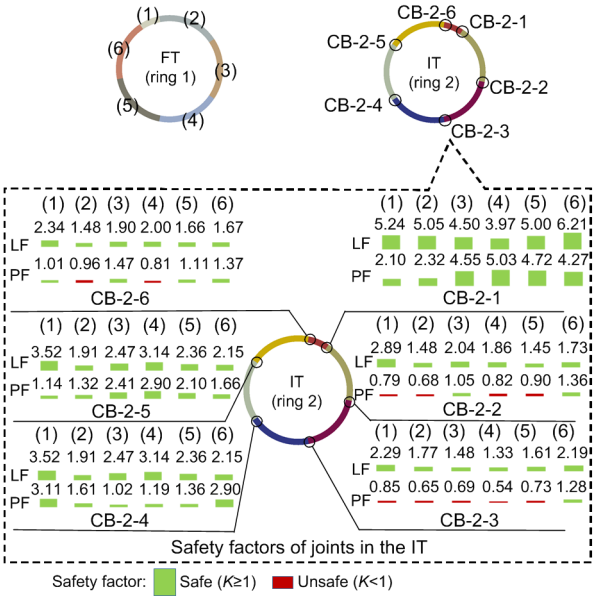

Fig. 12 Computing the safety factors of the joints in the IT in the Parallel case

(1)–(6) show six positions where local failure may occur. LF: only considering local failure; PF: considering progressive failure

When the two tunnels were arranged as overlaps, in the case Overlap-1, the joints in IT had sufficient redundancy of security (the safety factors ranged from 1.01 to 20.83). In the case Overlap-2, some joints in IT may go into the unsafe state. Fig. 14 shows the safety factors of the joints in the IT for Overlap-2. In LF, joint CB-1-5, which was located at the springline of the IT, and joint CB-1-3, which was located at the toe of the IT, were the two joints that had the smallest safety factors in most cases, and the smallest safety factor was 0.35. Meanwhile, the safety factors of joint CB-1-4 were smaller than 1 in most cases. In PF, joint CB-1-5 and joint CB-1-3 were the two joints that had the smallest safety factors in most cases, and the smallest safety factor was 0.28. In practical engineering, the joints located at the springline, toe, and invert of the IT should be enhanced.

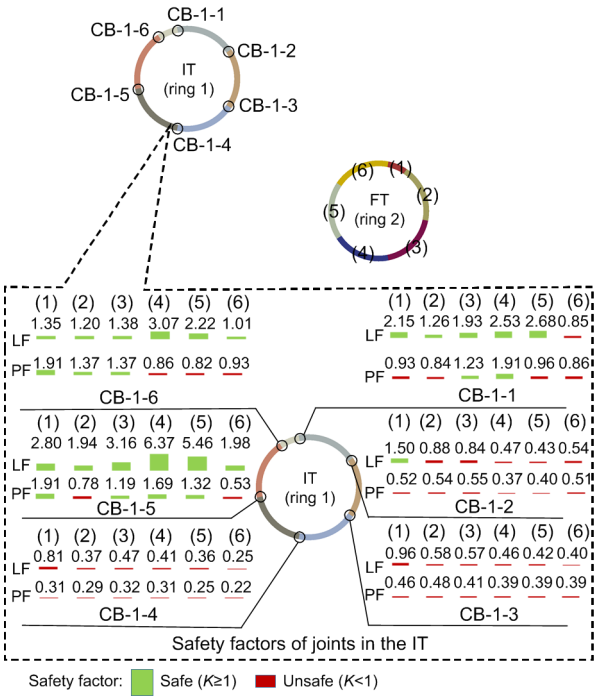

Fig. 13 Computing the safety factors of the joints in the IT in the case of Offset-2

The above study discussed the safety factors of the joints in the IT for cases of Parallel, Offset-1, Offset-2, Overlap-1, and Overlap-2. Herein, statistical analysis was carried out on 72 safety factors of the joints in the IT in each case. The probability for joints going into an unsafe state and the minimum safety factor were summarized in each case.

Fig. 15a shows the probability for joints going into an unsafe state in each case. Assume that the local failure occurred at each position in the FT with equal probability and that the circumstances also occurred with equal probability. The number of unsafe joints can statistically represent the probability that joints went into an unsafe state in the IT in each case. As shown in the figure, the maximum probability for

the joints in the IT to go into an unsafe state was 0.722 in the case of Offset-2. For Overlap-2, the joints in the IT also had a high probability of 0.583 to enter an unsafe state, although this probability was lower than that for Offset-2; for Parallel, the probability was 0.153, which was lower than that of the two above mentioned cases. For Offset-1 or Overlap-1, the probability that joints went into an unsafe state in the IT was nearly 0. These results can be described as follows: for offset and overlapping tunnels, the probability of the joints entering an unsafe state in the IT when the lower tunnel failed (case Offset-2 and case Overlap-2) was higher than that for the joints entering an unsafe state in the IT when the upper tunnel failed (Offset-1 and Overlap-1); the corresponding probability in the case of Parallel was intermediate.

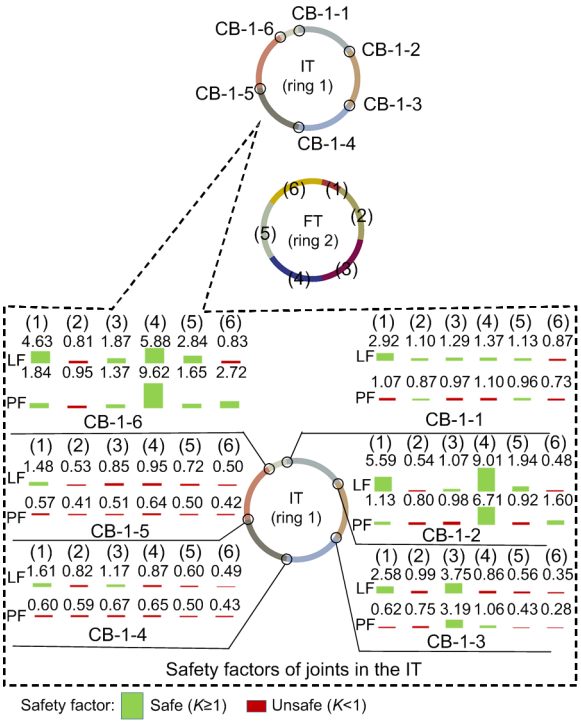

Fig. 14 Computing the safety factors of the joints in the IT in the case of Overlap-2

Fig. 15b shows the minimum safety factor, which was defined as the smallest safety factor among 72 safety factors of the joints in the IT in each case. It describes the largest degree that a joint leaves the envelope in the IT in each case. For Offset-2, the minimum safety factor was 0.22, which was the smallest among the different cases. This result means that the joint may leave the envelope to a large degree in this case. For Overlap-2, the minimum safety factor of the joints in the IT was 0.28, which was slightly higher than that of Offset-2. For Parallel, the minimum safety factor was 0.54. For Offset-1 and Overlap-1, the minimum safety factors were larger than 1. These results can be described as follows: for Offset-2, the joints in the IT should be enhanced substantially to ensure their safety. For Overlap-2, the minimum safety factor of the joints was slightly larger than that of Offset-2, and the material of the connecting bolts and concrete of the joints should be enhanced in the IT. In the case of Parallel, the minimum safety factor was twice as large as that of Offset-2, while the minimum safety factor remained less than 1. Hence, the enhancement of the joints in the IT should occur in the design stage. For Offset-1 and Overlap-1, the joints in the IT can always remain safe even if no enhancement is adopted.

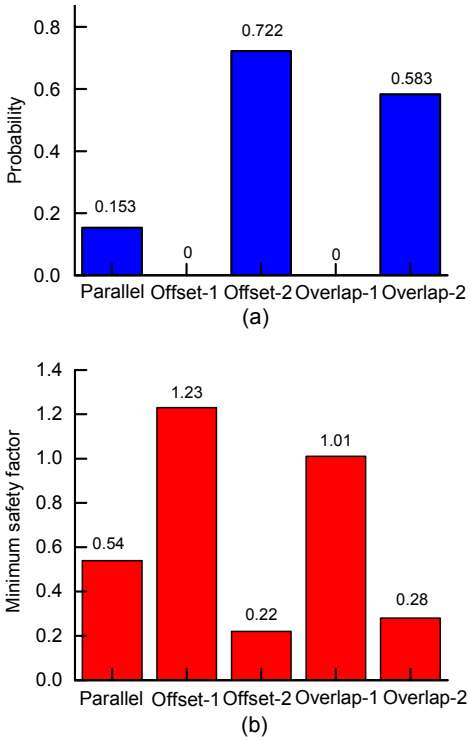

Fig. 15 Statistical analysis of the joints in the ITs in different cases

(a) Probabilities of joints that went into unsafe state in ITs in different cases; (b) Minimum safety factors of joints in ITs in different cases

Generally, from the perspective of the probability that the joints went into an unsafe state and the minimum safety factor, the safety factor of the joints in the IT can be evaluated among the different cases. For Offset-1 and Overlap-1, regardless of the position in which the FT failed and the circumstances, all joints in the IT were safe. This result demonstrated that a failure of the upper tunnel would have a slight influence on the joints of the lower tunnel. In the other three cases where some joints went into an unsafe state in the IT, the safety factor of the joints in the IT was the smallest for Offset-2, followed by Overlap-2. In Parallel, the safety factor of the joints in the IT was higher than those in the two cases mentioned. The above results can be explained as follows: as shown in Fig. 16, the shear strain was used to illustrate the development of the plastic zone. In the Parallel case, lateral unloading occurred near the IT, and horizontal extension occurred in the IT. For Overlap-2, the entire IT was located in the vertical unloading region, and vertical extension occurred in the IT. For Offset-2, the IT was located at the shear band of the FT where the soil had a large deformation gradient. Shear deformation occurred in the IT, and the joints were in the most adverse working state.

5 Conclusions

This paper introduced the CEL modelling technique and built a series of 2D models to study the failure propagation between two closely spaced tunnels. The following conclusions can be drawn based on the results of this study:

1. The sequence in which the joints in the IT went into an unsafe state mainly depended on the spatial relationships of the two tunnels, while different failure positions and different failure degrees in the FT may have a slight effect. In practical

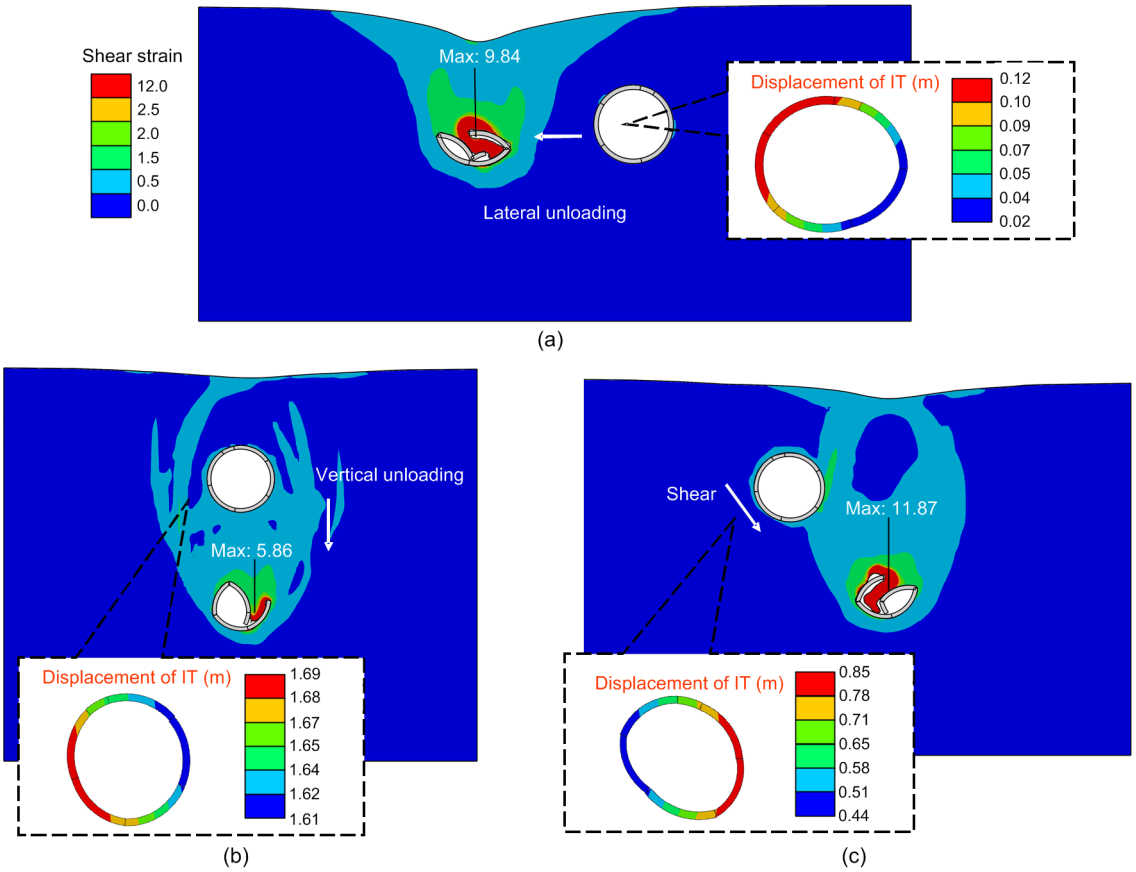

Fig. 16 Shear bands and the deformation of IT for cases of Parallel (a), Overlap-2 (b), and Offset-2 (c)
The deformation of the IT has been magnified by 10 times

engineering, if a spatial relationship is confirmed, the internal forces in the joints that first went into an unsafe state can be monitored to provide an early warning.

2. In overlapping and offsetting cases, the influence of the failure of the upper tunnel on the lower tunnel (Offset-1 and Overlap-1) was less than that of the lower tunnel on the upper tunnel (Offset-2 and Overlap-2). As a result, the joints in the upper tunnel should be enhanced.

3. In general, the joints in the IT were in a more dangerous situation when progressive failure occurred in the FT rather than only local failure. As a result, protecting the structure of the FT in a timely manner may have a positive effect on the safety of the joints in the IT.

4. Comparing the three cases in which the joints in the IT may go into an unsafe state (Parallel, Offset-2, and Overlap-2) shows that the safety factor of the joints in the IT was the smallest for Offset-2. The IT was located at the shear band of the FT where the soil had a large deformation gradient in the case of Offset-2. Shear deformation occurred in the IT, and the joints were in the most adverse working state. In practical engineering, the spatial relationship of offset tunnels is not recommended, and the joints in the upper tunnel should be enhanced.

Contributors

Gang ZHENG designed the research. Rui ZHU processed the corresponding data. Tian-qi ZHANG wrote the first draft of the manuscript. Ji-bin SUN, Jing-bo TONG, and Rui-kun WANG helped to organize the manuscript. Yu DIAO revised and edited the final version.

Conflict of interest

Gang ZHENG, Rui ZHU, Ji-bin SUN, Tian-qi ZHANG, Jing-bo TONG, Rui-kun WANG, and Yu DIAO declare that they have no conflict of interest.

References

Arrazola PJ, Özel T, 2010. Investigations on the effects of friction modeling in finite element simulation of machining. *International Journal of Mechanical Sciences*, 52(1):31-42. https://doi.org/10.1016/j.ijmecsci.2009.10.001

Atkinson JH, Potts DM, 1977. Stability of a shallow circular tunnel in cohesionless soil. *Géotechnique*, 27(2):203-215. https://doi.org/10.1680/geot.1977.27.2.203

Bi XL, Liu X, Wang XZ, et al., 2014. Experimental investigation on the ultimate bearing capacity of continuous-jointed segmental tunnel linings. *China Civil Engineering Journal*, 47(10):117-127 (in Chinese). https://doi.org/10.15951/j.tmgcxb.2014.10.028

Chambon P, Corté JF, 1994. Shallow tunnels in cohesionless soil: stability of tunnel face. *Journal of Geotechnical Engineering*, 120(7):1148-1165. https://doi.org/10.1061/(asce)0733-9410(1994)120:7(1148)

Cui T, 2017. Study on the Mechanism and Prevention of Progressive Failure of Shield Tunnel Induced by Local Failure. PhD Thesis, Tianjin University, Tianjin, China (in Chinese).

Dai XR, Wang JH, Fan YF, 2018. Issues of numerical simulation of the spudcan penetration based on CEL method. *Rock and Soil Mechanics*, 39(6):2278-2286 (in Chinese). https://doi.org/10.16285/j.rsm.2016.2142

Department of Emergency Management of Guangdong Province, 2019. Investigation Report on the Collapse of Metro Line 2 in Foshan, Guangdong Province (in Chinese). http://yjgl.gd.gov.cn/gk/zdlyxxgk/sgdcbg/content/post_2511537.html

Fang JH, Zhang ZH, Zhang JY, 2009. Application of artificial freezing to recovering a collapsed tunnel in Shanghai Metro No. 4 Line. *China Civil Engineering Journal*, 42(8):124-128 (in Chinese). https://doi.org/10.15951/j.tmgcxb.2009.08.003

Geng P, Tang R, Chen PL, et al., 2020. Research of mechanical model of shield tunnel's segment joint under the shearing effect. *Engineering Mechanics*, 37(3):157-166 (in Chinese). https://doi.org/10.6052/j.issn.1000-4750.2019.04.0213

He J, Ma JS, Wu DL, et al., 2019. Applications of CEL algorithmin soil large deformation simulation. *Computer Simulation*, 36(1):291-294 (in Chinese). https://doi.org/10.3969/j.issn.1006-9348.2019.01.060

Herle I, Gudehus G, 1999. Determination of parameters of a hypoplastic constitutive model from properties of grain assemblies. *Mechanics of Cohesive-Frictional Materials*, 4(5):461-486. https://doi.org/10.1002/(SICI)1099-1484(199909)4:5<461::A ID-C FM71>3.0.CO;2-P

HSE (Health and Safety Executive), 1996. Safety of New Austrian Tunneling Method (NATM) Tunnels. HSE, London, UK.

Huang ZK, Pitilakis K, Tsinidis G, et al., 2020. Seismic vulnerability of circular tunnels in soft soil deposits: the case of Shanghai metropolitan system. *Tunnelling and Underground Space Technology*, 98:103341. https://doi.org/10.1016/j.tust.2020.103341

Huang ZK, Pitilakis K, Argyroudis S, et al., 2021. Selection of optimal intensity measures for fragility assessment of circular tunnels in soft soil deposits. *Soil Dynamics and Earthquake Engineering*, 145:106724.

https://doi.org/10.1016/j.soildyn.2021.106724

Huo ZL, Yan Y, Li J, et al., 2016. Study of pipeline penetration in clay based on CEL. *China Offshore Platform*, 31(4):87-92. https://doi.org/10.3969/j.issn.1001-4500.2016.04.013

Jin YF, Yin ZY, Wu ZX, et al., 2018a. Identifying parameters of easily crushable sand and application to offshore pile driving. *Ocean Engineering*, 154:416-429. https://doi.org/10.1016/j.oceaneng.2018.01.023

Jin YF, Yin ZY, Wu ZX, et al., 2018b. Numerical modeling of pile penetration in silica sands considering the effect of grain breakage. *Finite Elements in Analysis and Design*, 144:15-29. https://doi.org/10.1016/j.finel.2018.02.003

Jin YF, Zhu BQ, Yin ZY, et al., 2019. Three-dimensional numerical analysis of the interaction of two crossing tunnels in soft clay. *Underground Space*, 4(4):310-327. https://doi.org/10.1016/j.undsp.2019.04.002

Jin Z, Yin ZY, Kotronis P, et al., 2019. Advanced numerical modelling of caisson foundations in sand to investigate the failure envelope in the *H-M-V* space. *Ocean Engineering*, 190:106394. https://doi.org/10.1016/j.oceaneng.2019.106394

Li XJ, Yan ZG, Wang Z, et al., 2015. Experimental and analytical study on longitudinal joint opening of concrete segmental lining. *Tunnelling and Underground Space Technology*, 46:52-63. https://doi.org/10.1016/j.tust.2014.11.002

Liu X, Huang XD, 2015. Experimental study of collapse capacity of straight joint segmental tunnel lining structure. *Chinese Journal of Rock Mechanics and Engineering*, 34(S2):3703-3714 (in Chinese). https://doi.org/10.13722/j.cnki.jrme.2015.0989

Liu X, Zhang CG, Zhang C, 2016. Investigation on the ultimate bearing capacity of longitudinal joints in segmental tunnel lining. *China Civil Engineering Journal*, 49(10): 110-122 (in Chinese). https://doi.org/10.15951/j.tmgcxb.2016.10.016

Lu M, Qin H, Zhu ZX, 2007. Introduction of shield running tunnel emergency repair of Shanghai rail rapid transit Line 9. *China Building Waterproofing*, (1):27-30 (in Chinese). https://doi.org/10.3969/j.issn.1007-497X.2007.01.009

Ng CWW, Sun HS, Lei GH, et al., 2015. Ability of three different soil constitutive models to predict a tunnel's response to basement excavation. *Canadian Geotechnical Journal*, 52(11):1685-1698. https://doi.org/10.1139/cgj-2014-0361

Niemunis A, Herle I, 1997. Hypoplastic model for cohesionless soils with elastic strain range. *Mechanics of Cohesive-Frictional Materials*, 2(4):279-299. https://doi.org/10.1002/(SICI)1099-1484(199710)2:4<279::AID-CFM29>3.0.CO;2-8

Qi L, Liu ZW, Xu H, et al., 2018. Comparative analysis of SPH and CEL methods used in submarine landslides. *Journal of Natural Disasters*, 27(6):180-185 (in Chinese). https://doi.org/10.13577/j.jnd.2018.0623

Qiu G, Grabe J, 2012. Numerical investigation of bearing capacity due to spudcan penetration in sand overlying clay. *Canadian Geotechnical Journal*, 49(12):1393-1407. https://doi.org/10.1139/t2012-085

Qiu G, Henke S, Grabe J, 2011. Application of a coupled Eulerian–Lagrangian approach on geomechanical problems involving large deformations. *Computers and Geotechnics*, 38(1):30-39. https://doi.org/10.1016/j.compgeo.2010.09.002

Seidenfuß T, 2006. Collapses in Tunneling. MS Thesis, Stuttgart University of Applied Sciences, Stuttgart, Germany (in German).

Wu ZX, Jin YF, Ji H, et al., 2017. Numerical simulation analysis of flat bottom pile drived into foundation of easily crushable sand. *Rock and Soil Mechanics*, 38(S2):330-336 (in Chinese). https://doi.org/10.16285/j.rsm.2017.S2.046

Yamamoto K, Lyamin AV, Wilson DW, et al., 2011. Stability of a single tunnel in cohesive–frictional soil subjected to surcharge loading. *Canadian Geotechnical Journal*, 48(12):1841-1854. https://doi.org/10.1139/T11-078

Yang L, 2011. The repair construction technology for a tunnel accident in a city. Proceedings of the 5th China's International Symposium on Tunneling, p.57-61 (in Chinese).

Yin ZY, Jin Z, Kotronis P, et al., 2018. Novel SPH SIMSAND-based approach for modeling of granular collapse. *International Journal of Geomechanics*, 18(11): 04018156. https://doi.org/10.1061/(ASCE)GM.1943-5622.0001255

Yin ZY, Wang P, Zhang FS, 2020. Effect of particle shape on the progressive failure of shield tunnel face in granular soils by coupled FDM-DEM method. *Tunnelling and Underground Space Technology*, 100:103394. https://doi.org/10.1016/j.tust.2020.103394

Zeng DY, He C, 2004. Numerical simulation of segment joint bending stiffness of metro shield tunnel. *Journal of Southwest Jiaotong University*, 39(6):744-748 (in Chinese). https://doi.org/10.3969/j.issn.0258-2724.2004.06.010

Zhang L, Su R, He C, et al., 2020. Full-scale experimental study on bending performance of segmental joints of large cross-section shield tunnel under pure compressive bending condition. *Tunnel Construction*, 40(7):997-1003 (in Chinese). https://doi.org/10.3973/j.issn.2096-4498.2020.07.008

Zhang TQ, 2016. Investigation on the Induced Surface Settlements, Tunnel Interaction Mechanisms and Control Countermeasures During the Construction of Two Parallel Shield Tunnels. PhD Thesis, Tianjin University, Tianjin, China (in Chinese).

Zheng G, Sun JB, Zhang TQ, et al., 2018. Eulerian finite

element model for stability analysis of circular tunnels in undrained clay. *Engineering Failure Analysis*, 91:216-224.
https://doi.org/10.1016/j.engfailanal.2018.04.022

Zheng G, Sun JB, Zhang TQ, et al., 2020. Mechanism and countermeasures of domino-like failure in underground pre-fabricated structures. *Engineering Failure Analysis*, 115(2):104603.
https://doi.org/10.1016/j.engfailanal.2020.104603

Appendix A Axial forces and bending moments of the segments in the IT

The axial forces and bending moments of the segments in the IT were extracted and are presented in Fig. A1. As clearly shown, all the internal forces in the segments were within the *M*-*N* envelope, indicating that the segments were safe in all cases.

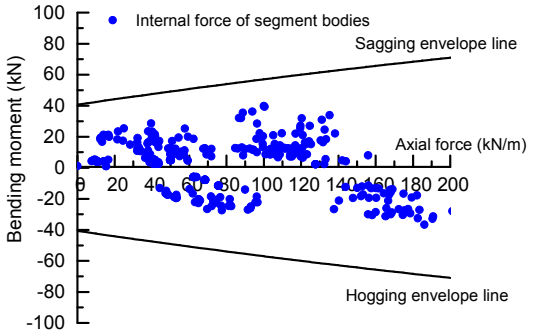

Fig. A1 Axial forces and bending moments of the segments in the IT